JACS
JOURNAL OF THE AMERICAN CHEMICAL SOCIETY
Article
Cite This: J. Am. Chem. Soc. 2017, 139, 14792-14799
pubs.acs.org/JACS

Ultrafast Delivery of Aggregation-Induced Emission Nanoparticles and Pure Organic Phosphorescent Nanocrystals by Saponin Encapsulation

Alexander Nicol,[†,⊥] Ryan T. K. Kwok,[†,⊥] Congping Chen,[‖] Weijun Zhao,[†,⊥] Ming Chen,[†,⊥] Jianan Qu,[‖] and Ben Zhong Tang*[,†,⊥,§]

[†]Division of Biomedical Engineering, Hong Kong Branch of Chinese National Engineering Research Center for Tissue Restoration and Reconstruction, Department of Chemistry, Institute for Advanced Study, Institute of Molecular Functional Materials and State Key Laboratory of Molecular Neuroscience, The Hong Kong University of Science and Technology (HKUST), Clear Water Bay, Kowloon, Hong Kong 999077, China

[⊥]HKUST-Shenzhen Research Institute No. 9 Yuexing First Road, South Area, Hi-tech Park, Nanshan, Shenzhen 518057, China

[‖]Department of Electronic and Computer Engineering, HKUST, Clear Water Bay Kowloon, Hong Kong 999077, China

[§]Guangdong Innovative Research Team, SCUT-HKUST Joint Research Laboratory, State Key Laboratory of Luminescent Materials and Devices, South China University of Technology, Guangzhou 510640, China

Supporting Information

ABSTRACT: Saponins are a class of naturally occurring bioactive and biocompatible amphiphilic glycosides produced by plants. Some saponins, such as α-hederin, exhibit unique cell membrane interactions. At concentrations above their critical micelle concentration, they will interact and aggregate with membrane cholesterol to form transient pores in the cell membrane. In this project, we utilized the unique permeabilization and amphiphilic properties of saponins for the intracellular delivery of deep-red-emitting aggregation-induced emission nanoparticles (AIE NPs) and pure organic room-temperature phosphorescent nanocrystals (NCs). We found this method to be biocompatible, inexpensive, ultrafast, and applicable to deliver a wide variety of AIE NPs and NCs into cancer cells.

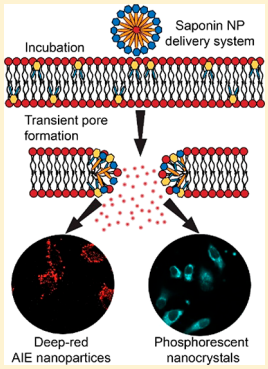

INTRODUCTION

Saponins are a naturally occurring group of amphiphilic sterol and triterpenoid glycosides found in the roots, bark, stems, leaves, and flowers of many plant species around the world. Saponins play a role in the defense system of plants and act as antimicrobial, antifungal, and insect-deterring agents.[1] The unique bioactivity of saponins has been known to humans indirectly for thousands of years. For example, the Yanomamö indigenous tribe of the Northern Amazon rainforest used the timbó plant, *Paullinia pinnata*, which contains high levels of saponin, as a shampooing and medicinal agent. In the absence of scientific reasoning, cultural evolution had allowed the Yanomamö tribe to find intelligent applications for saponins. With modern science, systematic studies have found an even wider range of applications for saponins, ranging from human cosmetics to agrochemical adjuvants.[2] An extensive literature base has shown that many of the biological effects of saponins are derived from their unique interactions with membrane components like cholesterol and phospholipids.[3] These interactions range from modulating membrane dynamics and interacting with membrane rafts to membrane permeabilization and membrane lysis.[4] The membrane permeabilization properties of saponins like α-hederin are particularly interesting because they offer an alternate biocompatible method to permeabilize live cells without the use of cytotoxic ionic surfactants like Triton X-100.[5] Figure S1 shows the chemical structure of α-hederin, which contains both a hydrophilic sugar part and a lipophilic steroid part. The first report of saponin membrane permeabilization was in 1962, when Bangham et al. observed hexagonal structures exclusively in cholesterol-containing planar membranes incubated with saponin.[6] They proposed a hexagonal micellar arrangement of saponins and cholesterol which created transient pores in the membrane plane.[7] This observation was later confirmed *ex vivo* when isolated cell membranes from human erythrocytes were treated with saponin and developed pores large enough to allow the diffusion of large 450 kDa proteins like ferritin into the cell.[8] Specific studies on α-hederin have revealed an even more elaborate concentration-dependent permeabilization mechanism based on aggregation with sterols and phospholipids which induce varying levels of membrane curvature. At

Received: August 21, 2017
Published: September 29, 2017

DOI: 10.1021/jacs.7b08710
J. Am. Chem. Soc. 2017, 139, 14792−14799

concentrations below the 0.03% critical micelle concentration (CMC), α-hederin monomers will intercalate and bind to sterols in the external monolayer.[9] At concentrations higher than the CMC, α-hederin will induce direct membrane pore formation and cause a loss of temporary membrane potential.[10] This cell membrane permeabilization mechanism is illustrated in Scheme 1. Simple yet effective nanoemulsion and nanoparticle drug delivery systems have been developed to utilize the unique membrane permeabilization properties of α-hederin and other saponins.[11−14] The main advantages of these system are their low cost, fast delivery times, and selective bioactivity.

Scheme 1. Cell Permeabilization Mechanism for the Ultrafast Delivery of Saponin Aggregation-Induced Emission Nanoparticles and Nanocrystals[a]

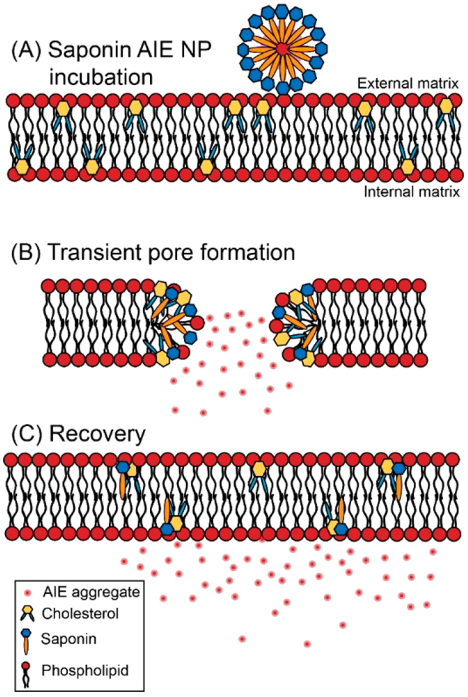

[a](A) Saponin AIE NPs interact with the cellular membrane by binding to cholesterol. (B) This will result in the formation of a transient pore, allowing the ultrafast delivery of the AIE NPs. (C) After a short recovery period the membrane integrity may be restored.

After recognizing the advantages of saponin delivery systems, we were eager to see whether it could be used to deliver some of the nonconventional luminogens developed in our laboratory into mammalian cells. Our specific interest was narrowed down to two unique cell-impermeable luminogens. The first systems include large molecular weight, highly conjugated, deep-red-emitting aggregation-induced emission nanoparticles (AIE NPs). AIE is a photophysical phenomenon observed in some rotor-containing fluorogenic molecules which are nonemissive when molecularly dissolved but highly emissive when aggregated.[15,16] This is caused by the restriction of intramolecular rotations.[17−19] Molecularly dissolved rotor-containing species are nonemissive because they undergo low-frequency motions leading to nonradiative decay. When such species are aggregated, these motions are blocked by intermolecular steric interactions, allowing bright fluorophore emission even in the solid state.[20] Deep-red- to near-infrared-emitting AIE NPs are particularly coveted for bioimaging because of their high imaging penetration depth, which avoids the autofluorescence emission band.[21,22] Deep-red-emissive NPs have found diverse bioimaging applications, ranging from multiphoton imaging to blood vesicle mapping.[23−25] AIE NPs' comparative advantage relative to other fluorescent systems comes from their remarkable high photostability, low cytotoxicity, and high brightness in the solid state owing to their strong AIE properties.[26] For this report we selected two deep-red AIE luminogens (AIEgens), 2,3-dicyano-5,6-di(4′-diphenylamino-biphenyl-4-yl)pyrazine (CAPP) and 2-(2,6-bis((*E*)-4-(bis(4′-(1,2,2-triphenylvinyl)-[1,1′-biphenyl]-4-yl)-amino)styryl)-4*H*-pyran-4-ylidene)malononitrile (TPE-TETRAD), as shown in Figure 1A and B, respectively.[27,28] Their

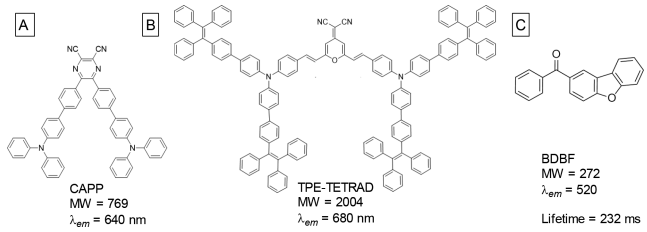

Figure 1. Chemical structure and properties for (A) CAPP, (B) TPE-TETRAD, and (C) BDBF. CAPP and TPE-TETRAD are both cell-impermeable deep-red-emitting AIEgens. BDBF can form pure organic room-temperature phosphorescent nanocrystals.

long emission wavelengths are primarily due to their unique donor−acceptor structure. TPE-TETRAD is a large TPE-containing AIEgen, whereas CAPP is relatively half the molecular weight and contains no TPE units. Both AIEgens are cell-impermeable due to their large molecular size and hydrophobic nature. To circumnavigate the issue of cell impermeability, many published investigations have used elaborate nanoparticle encapsulation and targeting strategies. However, the major drawbacks to these nanoparticle delivery strategies are their high cost, synthetic complexity, and long incubation times. A saponin delivery system for these deep-red-emitting AIE NPs would be of great benefit to reduce the cost and incubation time necessary for bioimaging.

The second system that we were interested to study for delivery with saponin was that of pure organic room-temperature phosphorescent nanocrystals (RTP NCs). A recent report by our group showed that it was possible to modulate the aggregation behaviors of arylphenones to suppress nonradiative decay to achieve efficient light emission and long lifetimes.[29,30] This was accomplished by tailoring the aromatic subunits in arylphenones to effectively tune the energy level and the orbital feature of the triplet exciton. Our results showed that pure organic phosphors with a balanced lifetime up to 0.23 s and efficiency up to 36% can be realized under ambient room-temperature conditions. Longer lifetimes, into the second regime, are highly favorable for bioimaging because, with a simple shutter delay, one can eliminate the interfering effects of autofluorescence.[31] Autofluorescence emission occurs in the nanosecond regime and can easily be separated from the millisecond emission lifetimes of phosphorescent imaging compounds.[32] However, bioimaging applications have not yet been realized with our pure organic NCs due to the inability of nanocrystals to permeate mammalian cells. A saponin delivery system for RTP NCs would be of great benefit, opening the possibility of phosphorescent lifetime imaging.[33]

DOI: 10.1021/jacs.7b08710
J. Am. Chem. Soc. 2017, 139, 14792−14799

RESULTS AND DISCUSSION

Preparation and Characterization of Saponin AIE NPs. Two different deep-red-emitting AIEgens (CAPP and TPE-TETRAD) were used to fabricate saponin AIE NPs following the procedure illustrated in Scheme 2. The first step involved

Scheme 2. Fabrication of Saponin AIE NPs

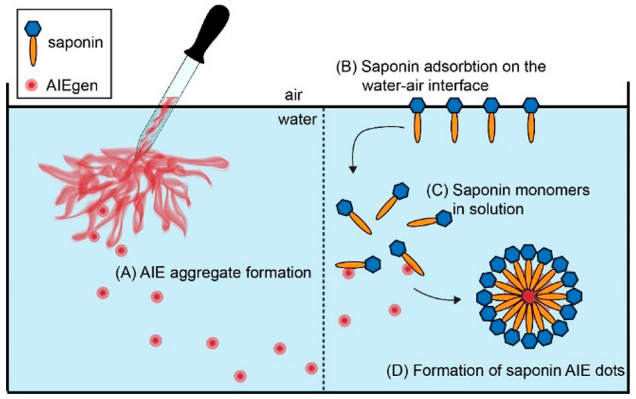

forming uniform AIE aggregates using a modified nanoprecipitation method. After 10 min of vigorous stirring, 20 μL of saponin (1 mg/mL) was added to both encapsulate and stabilize the AIE aggregates. The saponin concentration added was carefully selected to be above the 0.03% CMC. The saponin molecules readily self-assembled to form micelles in the aqueous solution due to their amphipathic structure consisting of both a sugar and a steroid moiety. The AIE aggregates were naturally encapsulated inside the saponin micelles due to their hydrophobic properties. The saponin AIE nanoparticles' size, shape, and polydispersity were analyzed using dynamic light scattering (DLS) and transmission electron microscopy (TEM) as show in Figure 2. CAPP saponin NPs

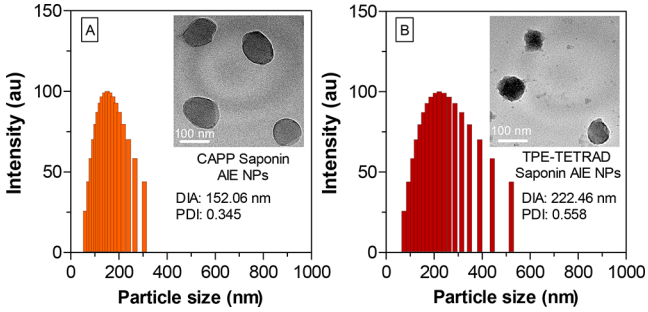

Figure 2. (A) Particle size distribution for saponin@CAPP and (B) saponin@TPE-TETRAD NPs measured by DLS. Inset: TEM images for both saponin AIE NPs. Scale bar = 100 nm (A) and 200 nm (B).

(saponin@CAPP) had a hydrodynamic diameter of 152 nm and a low polydispersity of 0.34. TPE-TETRAD saponin NPs (saponin@TETRAD) had a hydrodynamic diameter of 222 nm and a polydispersity of 0.55. The TEM results also confirmed that uniform spherical nanoparticles were formed. The larger size of saponin@TETRAD NPs can be attributed to the larger molecular size and higher hydrophobicity of TPE-TETRAD which translates to inherently larger aggregates. We found that the modified nanoprecipitation method yielded the smallest sized saponin AIE NPs.

Ultrafast Live Cell Imaging Using Deep-Red Saponin AIE NPs. Cytotoxicity evaluation is an important parameter to consider when developing a new delivery system. This is particularly critical for delivery strategies that involve membrane permeabilization or modulation. Previous reports have shown that strong ionic surfactants like Triton X-100 are highly toxic and cause irreversible DNA fragmentation and cell lysis.[3] To test whether these same negative effects would emerge using our saponin system, an MTT assay was conducted as shown in Figure 3. Remarkably, we found that

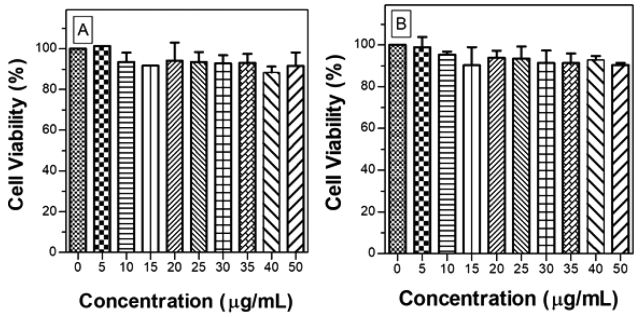

Figure 3. Cell viability assay of HeLa cervical cancer cells after staining with different concentrations of (A) saponin CAPP NPs and (B) saponin TPE-TETRAD NPs for 24 h at 37 °C. No significant difference was calculated between trials ($P < 0.05$).

both (A) saponin@CAPP NPs and (B) saponin@TPE-TETRAD NPs showed very little cytotoxicity up to 50 μg/mL after 24 h incubation. These results are also supported by Figure S2, showing that CAPP and TPE-TETRAD NPs without saponin encapsulation also have very low cytotoxicity. The high biocompatibility of this method depends on using a low concentration of saponin, just above the CMC, which allows the membrane permeabilization to be reversible. To further study the membrane modulation and delivery properties of the saponin NPs, HeLa cervical cancer cells were incubated with saponin@TPE-TETRAD NPs for various time intervals as depicted in Figure 4. Remarkably, even after just 30 s of incubation, we can observe the bright emission from TPE-TETRAD NPs within the HeLa cells. The emission intensity and uptake percent increase as the incubation time is increased,

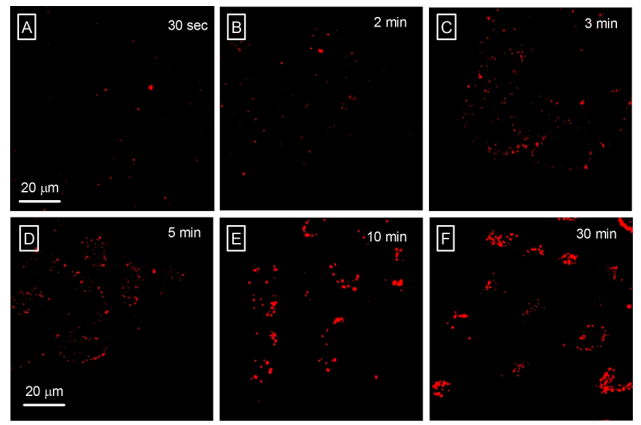

Figure 4. CLSM images of HeLa cervical cancer cells after incubation with 0.5 μg/mL of saponin@TPE-TETRAD NPs for (A) 30 s, (B) 2 min, (C) 3 min, (D) 5 min, (E) 10 min, and (F) 30 min. Scale bar = 20 μm for all images.

DOI: 10.1021/jacs.7b08710
J. Am. Chem. Soc. 2017, 139, 14792−14799

with an optimal incubation time calculated at 5 min. We also noticed that as the incubation time increased in Figure 5, the emission intensity increased and the cells condensed to what appear to be lysosome organelles.

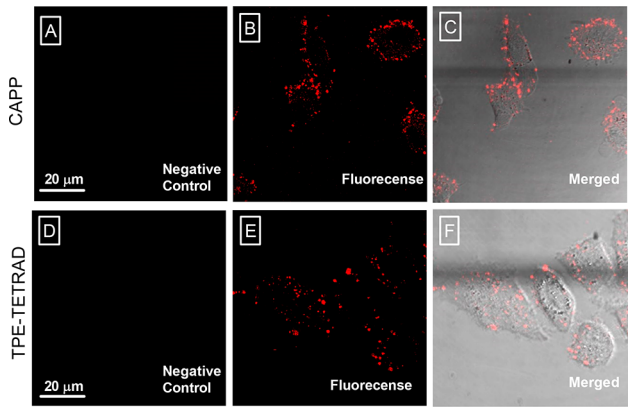

Figure 5. CLSM images of HeLa cervical cancer cells incubated with 0.5 μg/mL of (A) CAPP nanoaggregates, (B,C) saponin@CAPP NPs, (D) TPE-TETRAD nanoaggregates, or (E,F) saponin@TPE-TETRAD NPs for 5 min at 37 °C. Scale bar = 20 μm for all images.

A co-incubation study was performed, with results shown in Figure S3, to verify this by incubating 50 nM LysoTracker Green and 0.5 μg/mL of saponin@CAPP NPs for 30 min. A colocalization rate of over 37% was found indicating indeed some of the emission originated from the lysosome whereas most originated from the cytoplasm. We believe that the sequestration of CAPP over time in the lysosome is part of the cellular process of exocytosis.[34] Furthermore, some reports have suggested that cancer cells have higher lipid and cholesterol content on their membrane surfaces.[35] To test if this method had any selectivity to cancer cells, we incubated saponin@TPE-TETRAD NPs with noncancerous MDCK-II kidney cells and found similar uptake levels when compared to cancerous HeLa cells indicating that this method can be universally applied to both cancerous and noncancerous cell lines. The optimal incubation time was determined to be 5 min because of the combined advantages in mitigating toxicity and maximizing image quality. As shown in Figure 5A,D, without saponin encapsulation, neither CAPP nor TPE-TETRAD is able to enter HeLa cells.

However, with saponin encapsulation, saponin@CAPP NPs (Figure 5B,C) and saponin@TPE-TETRAD NPs (Figure 5E,F) were able to brightly stain HeLa cells in just 5 min. The image quality between saponin@TPE-TETRAD and saponin@CAPP is remarkably similar despite the latter being almost 100 nm larger in diameter. This can be attributed to the diffusion-based saponin delivery mechanism which is much less size specific than other delivery mechanisms which rely on endocytosis. The ultrafast 5 min imaging speed is orders of magnitude faster than any recently published AIE NP delivery systems which can often require up to 8 h incubation times.[36] Although many of the previously reported NP systems have high specificity and selectivity, long incubation times can be a critical barrier for their real-world clinical applications. Figure 6 shows a comprehensive comparison of the different effective staining times required for various AIE NP and conventional systems. Very few deep-red-emitting systems are reported to effectively stain cells in less than 30 min, which is ideal for

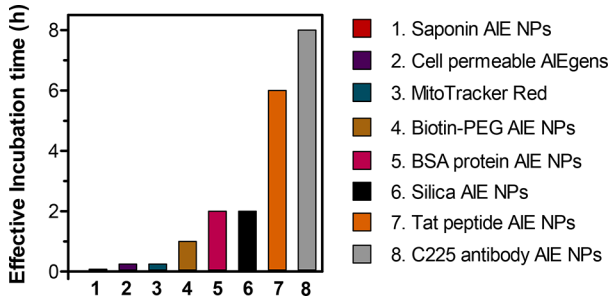

Figure 6. Effective staining time comparison between cell-permeable AIEgens, commercial fluorescent dyes, and various AIE NP delivery platforms. The effective incubation time was selected according the following references: cell-permeable AIEgens,[47] MitoTracker Red,[48] Biotin AIE NPs,[27] BSA protein NPs,[49] Silica AIE NPs,[50] Tat peptide AIE NPs,[23] and C225 antibody AIE NPs.[36]

clinical applications. This is because these systems rely on slow thermodynamically driven endocytosis mechanisms for cellular NP uptake. However, saponin delivery systems are able to temporarily permeabilize the membrane allowing for diffusion driven uptake. Diffusion-based uptake rather than the conventional endocytosis-based uptake is the main explanation for the ultrafast bioimaging process.

Ultrafast Live Cell Imaging Using Saponin RTP NCs. Our recent report showed that it was possible to modulate the aggregation behaviors of organic arylphenones to suppress nonradiative decay to achieve efficient light emission and long lifetimes.[29] 1-(dibenzo[*b*,*d*]furan-2-yl)phenylmethanone (BDBF) selected as the most promising RTP NC from this report due to its well-balanced lifetime of 0.23 s and emission efficiency of 36% under ambient room-temperature conditions. The long lifetime and high emission efficiency of BDBF made it a particularly attractive bioimaging and phosphorescent lifetime imaging probe. However, the BDBF NCs turned out to be highly cell impermeable and unable to enter HeLa cells as shown in Figure 7A,B.

Furthermore, we tried several PEG-based NP encapsulation strategies but were unsuccessful at delivering the BDBF NCs into HeLa cells. Saponin-encapsulated BDBF RTP NCs (saponin@NCs) were fabricated by a method similar to that used for the saponin AIE NPs where 20 μL of saponin (1 mg/mL) was added to 1 mg of BDBF NCs in 1 mL of PBS. As shown in Figure S5, uniformly sized saponin@NCs were formed with an effective diameter of 476.71 nm and a PDI of 0.158 as measured by DLS. SEM analysis revealed that the NC varied in size from 100 to 1000 nm. The wide distribution of NC size is an ongoing concern which we are trying to solve through new nanocrystallization methods. This is evident in the bioimaging results shown in Figure 7C, where HeLa cells were incubated for 5 min with saponin@NCs. When very minimal washing was used before imaging, one can clearly see highly emissive spots in the field of view. We suspect that these emissive spots are NCs which are too large to diffuse into the cell via the saponin induced permeabilization. The HeLa cells are likely stained with smaller sized BDBF NCs which are able to diffuse through the permeabilized membrane. When extensive washing was applied before imaging, one can clearly see that the large NCs have been washed away leaving only the remaining HeLa cells stained with saponin@NCs. In addition to being able to stain HeLa cells, the saponin@NCs also exhibited remarkably high photostability properties. As shown in Figure 8A, even after 110 confocal laser scanning microscope

DOI: 10.1021/jacs.7b08710
J. Am. Chem. Soc. 2017, 139, 14792−14799

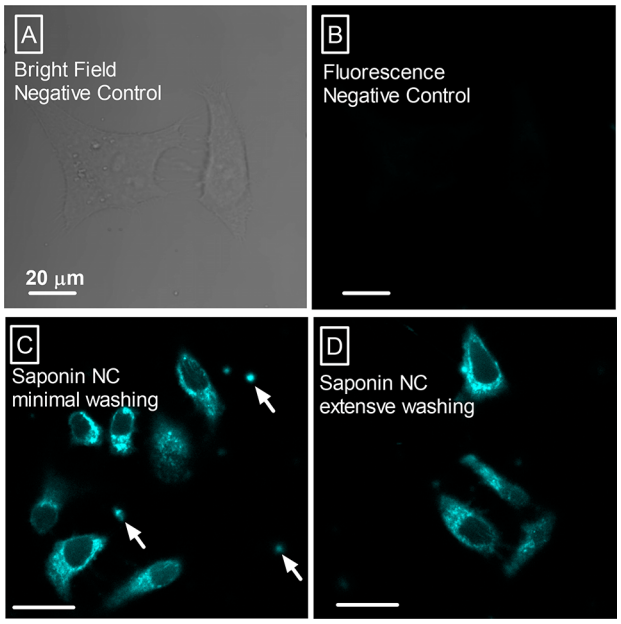

Figure 7. CLSM images of HeLa cells after 5 min incubation with (A,B) 1 μg/mL of pure nanocrystals or (C,D) 1 μg/mL of saponin @ NCs. Scale bar = 20 μm for all images.

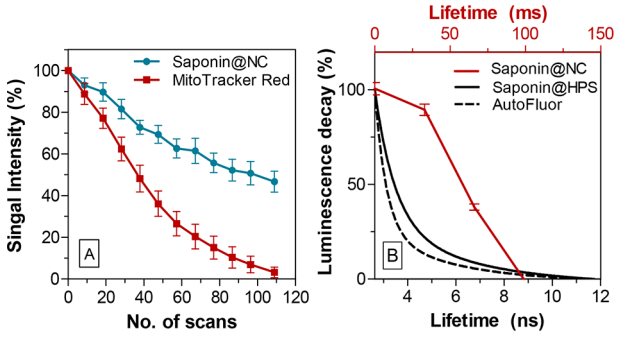

Figure 8. (A) Photostability comparison between saponin nanocrystals (blue) and MitoTracker Red (red) in HeLa with increasing number of CLSM scans at 80% laser power. (B) Normalized luminescence decay comparison between saponin@NCs, HPS, and cellular autofluorescence in HeLa cells. The top x-axis corresponds to the ms lifetime decay rate of the saponin@NCs whereas the bottom x-axis corresponds to the ns lifetime decay rates of HPS and autofluorecence.

(CLSM) scans at 80% laser power, the saponin@NCs still remained very emissive whereas conventional commercial photobleaching resistant dyes like MitoTracker Red became fully photobleached. This can be attributed to the AIE properties of the saponin@NCs which are capable of staying highly emissive in the solid crystalline state. Phosphorescent compounds are particularly attractive in bioimaging because with a simple shutter delay, one can eliminate the interfering effects of autofluorescence. Autofluorescence emission occurs in the ns regime and can easily be separated from ms emission lifetimes of phosphorescent imaging compounds. To demonstrate that BDBF saponin@NCs still retained its ms emission lifetime inside HeLa cells, a simple experiment was conducted as shown in Figure 8. First, the luminescence decay was recorded for just HeLa cells to collect an autofluorescence background signal. As shown in Figure 8, the autofluorescence signal quickly decays to 0% in around 10 ns. Hexaphenylsilole (HPS) was selected as a fluorescent dye reference because it has similar emission properties as BDBF and is also AIE active.[37] The luminescence decay of HPS is slightly slower than that of the autofluorescence signal but still decays to 0% in around 10 ns. However, the luminescence decay of BDBF saponin@NCs is significantly longer and reaches 0% in around 100 ms, which is 4 orders of magnitude longer than both HPS and autofluorescence. This makes saponin@NCs particularly attractive for bioimaging applications that require minimal autofluorescence and phosphorescent lifetime imaging.

CONCLUSION AND PROSPECTS

A saponin-based delivery method was presented for the intracellular delivery of deep-red-emitting AIE NPs and pure organic phosphorescent BDBF NCs. The unique permeabilization and amphiphilic properties of saponin allowed the successful delivery of large deep-red-emitting AIE nanoparticles in under 5 min, which is around 20 times faster than previously reported nanoparticle delivery systems. Furthermore, pure organic phosphorescent BDBF NCs were also successfully delivered to HeLa cells and showed persistent lifetimes up to 100 ms, which is 4 orders of magnitude longer than conventional dyes, and background autofluorescence. Our future work will focus on obtaining uniform NCs via new nanocrystallization methods and exploring their application in intracellular oxygen sensing using phosphorescent lifetime imaging.[38−40] We would also like to emphasize the versatility of saponin delivery systems, and we can foresee its application in delivering a wide range of other fluorescent materials. We also hope to explore more theranostic-based AIE saponin systems. For example, some avicin-type saponins were found to have selective pro-apoptotic activity in cancer cells by accelerating hydroperoxide-induced oxidation of mitochondrial endogenous NAD(P)H.[41,42] Saponins can also activate the mammalian immune system, leading to their potential use as vaccine adjuvants.[43] This has led to the formulation of saponin-adjuvanted immuno-stimulating complexes which induce both antibody and cellular immune responses with a broad range of vaccines in a variety of animal models.[44,45] Our future work will therefore be focused on leveraging the unique bioactivity of saponins with the favorable bioimaging properties of AIEgens.

EXPERIMENTAL SECTION

Materials. Saponin was purchased from Alfa Aesar, Inc. (USA). TPE-TETRAD, CAPP, and BDBF were either purchased from AIEgen Biotech, Inc. (Hong Kong) or synthesized according to our previous reports.[28,29] The synthetic starting materials were obtained from Sigma−Aldrich (St. Louis, USA). Cell culturing materials and MitoTracker Red were purchased from ThermoFisher Scientific (USA) including penicillin-streptomycin solution, Lysotracker Green, and 3-(4,5-dimethylthizaol-2-yl)-2,5-diphenyltetrazolium bromide (MTT). Dulbecco's Modified Eagle Medium (DMEM), modified essential medium (MEM), and MitoTracker Green were purchased from Invitrogen. Fetal bovine serum (FBS) and trypsin-EDTA solution were purchased from Life Technologies. Tetrahydrofuran (THF) and dichloromethane (DCM) were distilled from sodium benzophenone ketyl and calcium hydride under nitrogen, respectively. Milli-Q water purified via the Milli-Q Plus System (Millipore Corporation, United states). HeLa cervical cancer cells and MDCK-II noncancerous kidney cells were obtained from the American Type Culture Collection.

Characterization. The absorption spectra were recorded using a Shimadzu UV-2600 spectrometer. The emission spectra were recorded using a Perkin−Elmer LS 55 spectrofluorometer. The average particle size and the size distribution of the AIE NPs were measured by dynamic light scattering (DLS), using a 90Plus particle-size analyzer

DOI: 10.1021/jacs.7b08710
J. Am. Chem. Soc. 2017, 139, 14792−14799

(Brookhaven Instruments Co., USA) at a fixed angle of 90° and at room temperature. A Leica DMI 6000 fully motorized inverted microscope was used for CLSM and TPEF imaging. The morphology of the AIE NPs were investigated by SEM (JEM-2010F, JEOL, Japan). The lifetime and related data were measured on an Edinburgh FLSP920 fluorescence spectrophotometer equipped with a xenon arc lamp (Xe900), a microsecond flash lamp (uF900), a picosecond pulsed diode laser (EPL-375), a closed-cycle cryostate (CS202*I-DMX-1SS, Advanced Research Systems), and an integrating sphere (0.1 nm step size, 0.3 s integration time, five repeats), respectively.

Synthesis of TPE-TETRAD. TPE-TETRAD was synthesized on the basis of our previous report using the Knoevenagel condensation and Suzuki coupling reactions.[27] TPE-TETRAD is a dark red product and was purified by silica-gel column chromatography using hexane/dichloromethane as the eluent. TPE-TETRAD has good solubility in common organic solvents such as tetrahydrofuran, toluene, dichloromethane, and chloroform but is insoluble in water. All the compounds and intermediates were characterized by ^{1}H NMR, ^{13}C NMR, and high resolution mass spectrometry which confirmed their correct structures. ^{1}H NMR (400 MHz, $CDCl_3$), δ [ppm]: 7.56−7.43 (m, 20H), 7.39−7.34 (m, 16H), 7.33−7.00 (m, 66H), 6.67 (d, J = 16 Hz, 2H; pyran − CH =), 6.63 (s, 2H; pyran H); ^{13}C NMR (75 MHz, $CDCl_3$), δ [ppm]: 159.48, 149.98, 145.86, 143.77, 142.74, 141.21, 140.53, 139.07, 136.16, 131.58, 131.18, 128.69, 127.72, 126.15, 125.69, 122.11, 116.48, 115.15, 106.38, 53.41; HRMS (MALDI-TOF) for $C_{152}H_{105}N_4O$: m/z 2003.8378 (M^+, calculated 2004.5470).

Synthesis of CAPP. CAPP was prepated according to a previous report using a two-step procedure with a 96.8% yield.[28] The bright orange product was purified by silica-gel column chromatography. All the compounds and intermediates were characterized by ^{1}H NMR, ^{13}C NMR, and high resolution mass spectrometry which confirmed their correct structures. MALDI-TOF-MS: m/z 767.9 (M^+). ^{1}H NMR (400 MHz, $CDCl_3$), δ [ppm]: 7.67 (d, J = 8.5 Hz, 4H), 7.59 (d, J = 8.5 Hz, 4H), 7.49 (d, J = 8.7 Hz, 4H), 7.30−7.26 (m, 8H), 7.14−7.12 (m, 12H), 7.06 (t, 4H). ^{13}C NMR (100 MHz, $CDCl_3$), δ [ppm]: 154.8, 148.3, 147.4, 143.4, 133.5, 132.6, 130.4, 129.1, 127.7, 126.7, 124.8, 123.4, 123.3, 113.3.

Synthesis of BDBF. Anhydrous $AlCl_3$ (1.46 g, 11.0 mmol), benzoyl chloride (1.40 g, 10.0 mmol), and dibenzofuran (1.68 g, 10.0 mmol) were mixed at room temperature for 8 h and afforded the product as white powder. Yield: 2.41 g (89%). ^{1}H NMR (400 MHz, $CDCl_3$): δ [ppm]: 8.46 (d, J = 1.6 Hz, 1H), 7.99 (dd, J_1 = 8.8 Hz, J_2 = 2.0 Hz, 2H), 7.86 (dd, J_1 = 8.0 Hz, J_2 = 1.2 Hz, 2H), 7.66 (t, J = 9.2 Hz, 3H), 7.55 (m, 3H), 7.41 (t, J = 7.2 Hz, 1H). ^{13}C NMR (100 MHz, $CDCl_3$): δ [ppm]: 195.6, 157.9, 156.2, 137.5, 132.0, 131.7, 129.4, 129.2, 127.7, 127.3, 123.8, 123.1, 122.8, 122.7, 120.4, 111.3, 110.8. HRMS (MALDI-TOF) m/z: M^+ calculated 272.0837, found, 272.0839.

Fabrication of Saponin AIE Nanoparticles. The AIE NPs were prepared by adding 200 μL of TPE-TETRAD or CAPP (5 μg/mL in THF) dropwise to 1 mL of PBS in a scintillation vial. The mixture was vigorously stirred at room temperature for 10 min with a gentle stream of N_2 to help slowly evaporate the THF and form small dye aggregates. To make saponin AIE NPs, 20 μL of saponin (1 mg/mL) was subsequently added and stirred at room temperature for another 5 min. Both the saponin micelle AIE NPs and bare AIE NPs were immediatly characterized and used for experiments to limit any effects of aggregation.

Fabrication of Saponin RTP NCs. The saponin RTP NCs were prepared by adding 20 μL of saponin (1 mg/mL) to 1 mL of PBS in a scintillation vial and stirred at room temperature for 5 min. Then 1 mg of BDBF NCs was directly added to the vial and vigorously stirred at room temperature for another 10 min. Bare NCs were prepared in the same way excluding the initial addition of saponin. Both the saponin RTP NCs and bare NCs were immediatly characterized and used for experiments to limit any effects of aggregation.

Cell Culture. HeLa cervical cancer cells and MDCK-II non-cancerous kidney cells were provided by American Type Culture Collection. The HeLa cells were cultured in MEM while the MDCK-II cells were cultured in DMEM at 37 °C in a humidified incubator with 5% CO_2. Both culture mediums contained 10% heat-inactivated FBS 100 μg/mL penicillin and 100 μg/mL streptomycin. Before experiment, the cells were precultured until confluence was reached.

Cell Imaging. MDCK-II or HeLa cells were grown overnight on a 35 mm Petri dish with a coverslip. The live cells were stained with either the saponin AIE NPs or saponin RTP NCs at a working concentration of 0.5 μg/mL for 5 min at 37 °C. Before imaging on the confocal microscope, the cells were washed with three times with PBS. The treated coverslip was then mounted in standard mounting media and imaged using a fluorescent microscope (Leica DMI 6000). The excitation wavelength was 488 nm for the saponin AIE NPs and 405 nm for the saponin RTP NCs. For saponin TPE-TETRAD, a 600−750 nm emission filter was used. For saponin CAPP, a 600−700 nm emission filter was used. For saponin RTP NCs, a 500−550 nm emission filter was used. MitoTracker Red was used as directed by Thermo Fisher Scientific for all imaging experiments. When comparing the staining efficiency between MDCK-II and HeLa cell lines, the laser power was held constant at 80% as well as all other laser parameters (digital gain and offset) to provide an accurate comparison. To study the photostability of saponin BDBF NCs and MitoTracker Red in live HeLa cells, CLSM images were recorded at 2 s intervals with an excitation wavelength of 405 nm at 80% laser power. The fluorescence intensity of each image was analyzed using the Image Pro Plus software for each scan. The photostability of saponin BDBF NCs and MitoTracker Red was expressed by I/I_0, where I_0 is the initial fluorescence intensity and I is the fluorescence intensity after each subsequent scan. The data were obtained from replicated experiments (n = 20).

Cytotoxicity Study. MTT assays were used to evaluate the cytotoxicity of saponin TPE-TETRAD NPs, TPE-TETRAD aggregates, saponin CAPP NPs, and CAPP aggregates to HeLa cancer cells. The HeLa cells were seeded on 96-well plates (Costar, IL, USA) at a density of 1×10^4 cells cells/well. The cells were exposed to a series of doses of each sample (0−50 μg/mL) in culture medium at 37 °C. After 24 h incubation, 10 μL of freshly prepared MTT solution (5 mg/mL in PBS) was added into each well. After 4 h incubation, 100 μL of solubilizing solution containing 10% SDS and 0.01 M HCl was added to dissolve the purple MTT dye crystals. After 4 h incubation, the absorbance of MTT at 595 nm was monitored using a Perkin−Elmer Victor plate reader. Cell viability was expressed by the ratio of absorbance of the cells incubated with each AIE NP sample to that of cells incubated with culture medium only. The data were obtained from replicate experiments (n > 3).

Fluorescent Lifetime Imaging. The fluorescence lifetime imaging measurement of NADH autofluorescence and HPS fluorescence was conducted by using a home-built two-photon microscope. Briefly, a femtosecond Ti:sapphire laser (Chameleon Ultra II, Coherent) was tuned at 760 nm for two photon excitation. The emission was collected in the backward direction and separated from the excitation light by a dichroic mirror (FF665-Di02, Semrock). The fluorescence was selected out by a bandpass filter (NADH, FF02-447/60-25, Semrock; HPS, FF03-525/50-25, Semrock) before recorded by a single-channel hybrid detector and TCSPC module (HPM-100 40 and SPC-150, Becker & Hickl GmbH).

Phosphorescent Imaging. A custom-built time-resolved spectroscopic imaging system was used for this study.[46] A 473 nm laser (SDL-473-100T, Dream Lasers Technology) uniformly illuminated the sample using a 25× objective (XLPLN25XWMP2, Olympus). The phosphorescent emission was collected using the same objective through 525/550 nm band-pass filter and recorded with a CCD camera (pixelfly vga, PCO).

■ ASSOCIATED CONTENT

Supporting Information

The Supporting Information is available free of charge on the ACS Publications website at DOI: 10.1021/jacs.7b08710.

Supporting figures with information on important control experiments and characterization data: Figure S1, chemical structure of α-hederin; Figure S2, cell

DOI: 10.1021/jacs.7b08710
J. Am. Chem. Soc. 2017, 139, 14792−14799

viability assays of HeLa cervical cancer cells after staining with different concentrations of CAPP and TPE-TETRAD nanoaggregates; Figure S3, colocalization study with LysoTracker Green and saponin@CAPP NPs; Figure S4 shows CLSM images of MDCK-II kidney cells stained with CAPP@saponin; Figure S5, particle size distribution for saponin@NC measured by DLS and SEM image; Figure S6, photophysical characterization data; Figure S7, photostability of saponin@TPE-TETRAD AIE NPs in HeLa cells with increasing number of laser scans at 488 nm; Figure S8, long-term colloidal stability of various AIE NPs in different media (PDF)

AUTHOR INFORMATION

Corresponding Author

*tangbenz@ust.hk

ORCID

Alexander Nicol: 0000-0003-2945-683X
Ryan T. K. Kwok: 0000-0002-6866-3877
Ben Zhong Tang: 0000-0002-0293-964X

Notes

The authors declare no competing financial interest.

ACKNOWLEDGMENTS

This work was partially supported by the Innovation and Technology Commission (ITC, CNERC14SC01), the National Basic Research Program of China (973 Program; 2013CB-834701 and 2013CB834702), the University Grants Committee of Hong Kong (AoE/P-03/08), and the Research Grants Council of Hong Kong (16301614, 16305015, 16308016, N_HKUST604/14, and A-HKUST605/16). B.Z.T. is also grateful for the support from the Guangdong Innovative Research Team Program of China (201101C0105067115) and the Science and Technology Plan of Shenzhen (JCYJ2016-02229205601482). A.N. recognizes support from the Hong Kong Ph.D. Fellowship Program.

REFERENCES

(1) Barr, I.; Sjölander, A.; Cox, J. *Adv. Drug Delivery Rev.* **1998**, *32*, 247.
(2) Chapagain, B. P.; Wiesman, Z. *J. Agric. Food Chem.* **2006**, *54*, 6277.
(3) Izzi, A.; Benie, T.; Thieulant, M. L.; Men-Olivier, L.; Duval, J. *Planta Med.* **1992**, *58*, 229.
(4) Lorent, J. H.; Quetin-Leclercq, J.; Mingeot-Leclercq, M. P. *Org. Biomol. Chem.* **2014**, *12*, 8803.
(5) Dayeh, V. R.; Chow, S. L.; Schirmer, K.; Lynn, D. H.; Bols, N. C. *Ecotoxicol. Environ. Saf.* **2004**, *57*, 375.
(6) Bertaud, W. S.; Hedley, R. H. *Nature* **1963**, *200*, 89.
(7) Wassler, M.; Jonasson, I.; Persson, R.; Fries, E. *Biochem. J.* **1987**, *247*, 407.
(8) Seeman, P.; Cheng, D.; Iles, G. H. *J. Cell Biol.* **1973**, *56*, 519.
(9) Lorent, J.; Lins, L.; Domenech, Ò.; Quetin-Leclercq, J.; Brasseur, R.; Mingeot-Leclercq, M. P. *Langmuir* **2014**, *30*, 4556.
(10) Lorent, J.; Le Duff, C. S.; Quetin-Leclercq, J.; Mingeot-Leclercq, M.-P. *J. Biol. Chem.* **2013**, *288*, 14000.
(11) Ozturk, B.; Argin, S.; Ozilgen, M.; McClements, D. J. *J. Food Eng.* **2014**, *142*, 57.
(12) Skene, C. D.; Sutton, P. *Methods* **2006**, *40*, 53.
(13) Sjölander, A.; Cox, J. C. *Adv. Drug Delivery Rev.* **1998**, *34*, 321.
(14) Pillion, D. J.; Recchia, J.; Wang, P.; Marciani, D. J.; Kensil, C. R. *J. Pharm. Sci.* **1995**, *84*, 1276.
(15) Luo, J.; Xie, Z.; Lam, J. W.; Cheng, L.; Chen, H.; Qiu, C.; Kwok, H. S.; Zhan, X.; Liu, Y.; Zhu, D.; Tang, B. Z. *Chem. Commun.* **2001**, *381*, 1740.
(16) Mei, J.; Leung, N. L. C.; Kwok, R. T. K.; Lam, J. W. Y.; Tang, B. Z. *Chem. Rev.* **2015**, *115*, 11718.
(17) Hong, Y.; Lam, J. W. Y.; Tang, B. Z. *Chem. Commun.* **2009**, *29*, 4332.
(18) Mei, J.; Hong, Y.; Lam, J. W. Y.; Qin, A.; Tang, Y.; Tang, B. Z. *Adv. Mater.* **2014**, *26*, 5429.
(19) Wang, H.; Zhao, E.; Lam, J. W. Y.; Tang, B. Z. *Mater. Today* **2015**, *18*, 365.
(20) Ding, D.; Li, K.; Liu, B.; Tang, B. Z. *Acc. Chem. Res.* **2013**, *46*, 2441.
(21) Luo, S.; Zhang, E.; Su, Y.; Cheng, T.; Shi, C.; et al. *Biomaterials* **2013**, *34*, 2244.
(22) Feng, G.; Kwok, R. T. K.; Tang, B. Z.; Liu, B. *Appl. Phys. Rev.* **2017**, *4*, 021307.
(23) Li, K.; Qin, W.; Ding, D.; Tomczak, N.; Geng, J.; Liu, R.; Liu, J.; Zhang, X.; Liu, H.; Liu, B.; Tang, B. Z. *Sci. Rep.* **2013**, *3*, 1150.
(24) Liang, J.; Tang, B. Z.; Liu, B. *Chem. Soc. Rev.* **2015**, *44*, 2798.
(25) Shao, A.; Xie, Y.; Zhu, S.; Guo, Z.; Zhu, S.; Guo, J.; Shi, P.; James, T. D.; Tian, H.; Zhu, W. H. *Angew. Chem.* **2015**, *127*, 7383.
(26) Leung, C. W. T.; Hong, Y.; Chen, S.; Zhao, E.; Lam, J. W. Y.; Tang, B. Z. *J. Am. Chem. Soc.* **2013**, *135*, 62.
(27) Nicol, A.; Qin, W.; Kwok, R. T. K.; Burkhartsmeyer, J. M.; Zhu, Z.; Su, H.; Luo, W.; Lam, J. W. Y.; Qian, J.; Wong, K. S.; Tang, B. Z. *Chem. Sci.* **2017**, *8*, 4634.
(28) Chen, S.; Xu, X.; Liu, Y.; Yu, G.; Sun, X.; Qiu, W.; Ma, Y.; Zhu, D. *Adv. Funct. Mater.* **2005**, *15*, 1541.
(29) Zhao, W.; He, Z.; Lam, J. W. Y.; Zhao, W.; He, Z.; Lam, J. W. Y.; Peng, Q.; Ma, H.; Shuai, Z.; Bai, G.; et al. *Chem* **2017**, *1*, 592.
(30) Thilagar, P.; Mukherjee, S. *Chem. Commun.* **2015**, *51*, 10988.
(31) Zhao, Q.; Huang, C.; Li, F. *Chem. Soc. Rev.* **2011**, *40*, 2508.
(32) Kumar, R.; Ohulchanskyy, T. Y.; Roy, I.; Gupta, S. K.; Borek, C.; Thompson, M. E.; Prasad, P. N. *ACS Appl. Mater. Interfaces* **2009**, *1*, 1474.
(33) Lv, W.; Yang, T.; Yu, Q.; Zhao, Q.; Zhang, K. Y.; Liang, H.; et al. *Adv. Sci.* **2015**, *2* (10), 1500107.
(34) Schmoranzer, J.; Goulian, M.; Axelrod, D.; Simon, S. M. *J. Cell Biol.* **2000**, *149*, 23.
(35) Li, Y. C.; Park, M. J.; Ye, S.; et al. *Am. J. Pathol.* **2006**, *168*, 1107.
(36) Gao, M.; Su, H.; Lin, G.; Li, S.; Yu, X.; Qin, A.; Zhao, Z.; Zhang, Z.; Tang, B. Z. *Nanoscale* **2016**, *8*, 15027.
(37) Zhao, Z.; He, B.; Tang, B. Z. *Chem. Sci.* **2015**, *6*, 5347.
(38) Kasai, H.; Nalwa, H. S.; Baba, K.; Kasai, H.; Fang, P. H.; Bai, P.; Botzung-appert, E.; Silicon, M.; Fang, P. H.; Huan, Z.; Tsuboi, Y.; Akita, H.; Kim, H.; Hayashi, S.; Yamamoto, K. *Jpn. J. Appl. Phys.* **1996**, *35*, L221.
(39) Howard, S. S.; Straub, A.; Horton, N. G.; Kobat, D.; Xu, C. *Nat. Photonics* **2012**, *7*, 33.
(40) Botchway, S. W.; Haycock, J. W.; Williams, J. A. G.; Weinstein, J. A.; et al. *Chem. Sci.* **2014**, *5*, 879.
(41) Lemeshko, V. V; Haridas, V.; Quijano, J. C.; Gutterman, J. U. *Arch. Biochem. Biophys.* **2006**, *454*, 114.
(42) Haridas, V.; Higuchi, M.; Jayatilake, G. S.; Bailey, D.; Mujoo, K.; Blake, M. E.; Arntzen, C. J.; Gutterman, J. U. *Proc. Natl. Acad. Sci. U. S. A.* **2001**, *98*, 5821.
(43) Morein, B.; Sundquist, B.; Höglund, S.; Dalsgaard, K.; Osterhaus, A. *Nature* **1984**, *308*, 457.
(44) Pearse, M. J.; Drane, D. *Adv. Drug Delivery Rev.* **2005**, *57*, 465.
(45) Ronnberg, B.; et al. *Vaccine* **1995**, *13*, 1375.
(46) Hirvonen, L. M.; Festy, F.; Suhling, K. *Opt. Lett.* **2014**, *39*, 5602.
(47) Yu, C. Y. Y.; Zhang, W.; Kwok, R. T. K.; Leung, W. T.; Lam, J. W. Y.; Tang, B. Z. *J. Mater. Chem. B* **2016**, *4*, 2614.
(48) Invitrogen Molecular Probes, MitoTracker Mitochondrion Selective Probes, 2008.
(49) Qin, W.; Ding, D.; Liu, J.; Yuan, W. Z.; Hu, Y.; Liu, B.; Tang, B. Z. *Adv. Funct. Mater.* **2012**, *22*, 771.

DOI: 10.1021/jacs.7b08710
J. Am. Chem. Soc. 2017, 139, 14792−14799

(50) Mahtab, F.; Yu, Y.; Lam, J. W. Y.; Liu, J.; Zhang, B.; Lu, P.; Zhang, X.; Tang, B. Z. *Adv. Funct. Mater.* **2011**, *21*, 1733.

DOI: 10.1021/jacs.7b08710
J. Am. Chem. Soc. 2017, 139, 14792−14799